Int. J. Electrochem. Sci., 6 **(2011)** 4614 - 4627

International Journal of
ELECTROCHEMICAL
SCIENCE
www.electrochemsci.org

Electrochemical Behaviour of AISI 316 Austenitic Stainless Steel in Acidic Media Containing Chloride Ions

Y. Ait Albrimi[1], *A. Eddib*[1], *J. Douch*[1], *Y. Berghoute*[1], *M. Hamdani*[1,*], *R.M. Souto*[2]

[1] Laboratoire de Chimie Physique, Faculté des Sciences, Université Ibn Zohr, B.P. 8106, Cité Dakhla, Agadir, Maroc.
[2] Department of Physical Chemistry, University of La Laguna, E-38205 La Laguna (Tenerife, Canary Islands), Spain.
[*]E-mail: hamdani.mohamed@gmail.com

Received: 24 December 2010 / *Accepted:* 13 June 2011 / *Published:* 1 October 2011

The electrochemical behaviour of AISI 316 austenitic stainless steel (SS) was investigated in deaerated hydrochloric and sulphuric acid solutions using the open-circuit potential, cyclic voltammetric and chronoamperometric techniques. Enhanced corrosion of steel samples occurred with bigger HCl concentrations, as the potential range of passivity was shortened and both the pitting (E_{pit}) and the protection potentials (E_{prot}) became less noble. Conversely, the SS electrodes exhibited a greater corrosion resistance in solutions containing sulphuric acid of the same concentration. The aggressive effect of chloride ions towards steel corrosion was also investigated through controlled additions of NaCl to both electrolytic media and the analysis of the corresponding effects on the shape of the voltammetric curves. Chronoamperometric measurements run by setting different potential values to steel electrodes allowed the determination of the induction time for pit initiation, and the rates of pit nucleation and pit growth.

Keywords: Pitting corrosion, AISI 316 stainless steel, hydrochloric and sulphuric acids, chloride ions, pit nucleation.

1. INTRODUCTION

Austenitic stainless steels are widely used in industrial applications due to their strength, corrosion resistance, mechanical workability, and excellent electrical and thermal conductivities. Among them, AISI 316 stainless steel is of great practical interest because it is employed in pharmaceutical, petrochemical, offshore drilling marine shipping, water desalination, etc. AISI types 304 and 316 stainless steels are used to handle very diluted acid at low temperature [1].

The high corrosion resistance of this material arises from the formation of a passive layer on its surface.

Additionally, chromium content in the steel enhances its corrosion resistance. The passive film is constituted by an iron and chromium oxy-hydroxide layer and water containing-compounds which is formed at the metal/solution interface, and an underlying film formed by chromium oxide [2]. However, under certain circumstances, the passive state may be lost, and most stainless steel-based equipment failures are caused by pitting corrosion due to chloride ions [3-5].

Hydrochloric acid (next to sea water) remains the main source of the aggressive chloride ions. Pitting corrosion is one of the most dangerous forms of localized corrosion especially for steels in chloride media [6]. On the other hand, sulphuric acid is very corrosive for stainless steels too, and constitutes one of the basic raw materials encountered in the chemical industry. Despite the number of publications about stainless steel corrosion and passivation, the kinetics of the various complex processes involved has been investigated less extensively in concentrated solutions of these acids. Therefore, it is interesting both from the fundamental and practical standpoint to study the influence of acidity, chloride and sulphate ions on those processes. The presence of such ions imposes the use of inhibitors to avoid destruction of either the material surface or the passive layer in contact with the aggressive solution.

The adsorption of the inhibitor at the interface hinders the physical contact of chloride ions with the metal-solution interface.

In the present investigation, the corrosion behaviour of AISI 316 stainless steel exposed to either hydrochloric or sulphuric acid solutions has been investigated with special focus on the characterization of the pitting susceptibility of the steel in these environments. The influence of various factors such as the nature of the acidic media and its concentration, potential cycling, potential scan rate, and the addition of Cl^- ions were considered. Work is in progress at our laboratory to investigate the inhibition of SS corrosion employing natural non-toxic inhibitors.

2. EXPERIMENTAL METHODS

Austenitic stainless steel AISI 316 (Goodfellow, Cambridge, UK) supplied as plates has been used. Table 1 provides its nominal chemical composition as given by the supplier.

Table 1. Chemical composition of the AISI 316 austenitic stainless steel.

Elements	C	Mn	Si	Cr	Ni	Mo	P	S	N	Fe
wt%	0.08	2	0.75	18	10	2	0.045	0.03	0.1	balance

Plates of stainless steel were cut to dimensions 1 cm × 2 cm × 0.1 cm. The surface was ground employing a gradual sequence of emery papers of different grit sizes, namely 400, 600, 800, 1000, 1200 and 1500 grades. The ground specimen was rinsed, cleaned in an ultrasonic bath successively in twice-distilled water and in absolute ethanol, for 10 min each, and finally dried in air. All chemicals used in this work (namely HCl, H_2SO_4, NaCl) were reagent grade. Selected concentrations of hydrochloric or sulphuric acid were prepared by dilution of the corresponding concentrated solutions using twice-distilled water.

Electrochemical studies were carried out in a conventional three-electrode single-compartment pyrex glass cell (Model 499/GC pyrex cup, 70 ml volume, with the cover model 497/MH Moplen head provided with 5 openings). Steel plates were used as the working electrodes by putting only one side of the specimen in contact with the electrolyte (2 cm^2).

The remaining sides were covered with a non-reactive and non-conductive varnish. The electrical contact with the test electrode was made using a crocodile clip attached on a small strip of the plate.

The potential of the working electrode was measured against a saturated calomel electrode (SCE) (0.240V vs SHE). The SCE was connected through a KCl-containing agar-agar salt bridge, the tip of which was placed as close as possible to the surface of the working electrode in order to minimize the solution resistance between the test and reference electrodes. The counter electrode was an 8 cm^2 platinum plate.

The electrolyte volume was 50 ml, and it was deaerated by purging N_2 for 20 min prior to the measurements. When the addition of NaCl to the test electrolyte was considered, the desired amount of salt was added directly to the stirred electrolyte.

The electrochemical measurements were performed using a computerized potentiostatic electrochemical set Voltalab PRZ 100 (Radiometer-Analytical). The corrosion behaviour of the stainless steel was investigated in different HCl and H_2SO_4 aqueous solutions, at room temperature, using open-circuit potential (OCP), potentiodynamic polarization and chronoamperometric techniques. A new specimen was used for each run.

3. RESULTS AND DISCUSSION

3.1. Open-circuit potential

The evolution of the open-circuit potential (OCP) values recorded for AISI 316 austenitic stainless steel specimens in 0.1 N HCl and in 0.1 N H_2SO_4 are plotted in Fig. 1.

As it can be seen, the OCP values decreased abruptly and reached the steady-state value of -0.35 V_{SCE} in 0.1 N HCl and of -0.30 V_{SCE} in 0.1 N H_2SO_4. The time taken for the attainment of the steady-state was approximately 30 min. The shift of potential towards more negative values in hydrochloric acid solution indicates the enhancement of steel's corrosion susceptibility compared to its behaviour in sulphuric acid solution.

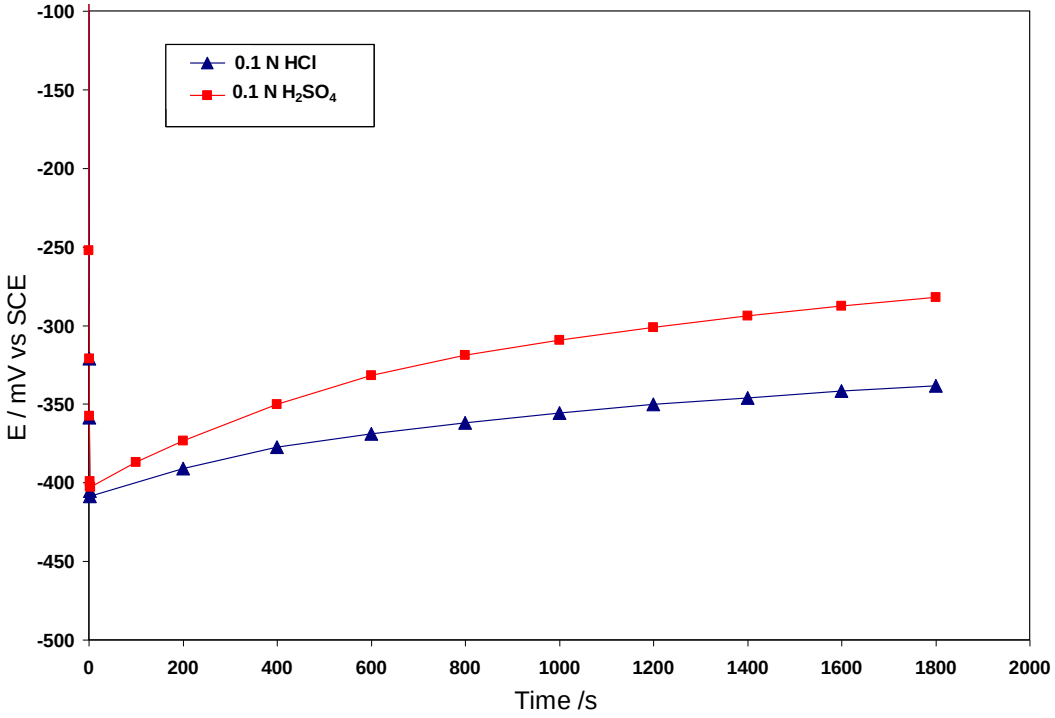

Figure 1. Time course of the open–circuit potential (OCP) values measured for AISI 316 electrodes immersed in 0.1 N HCl and in 0.1 N H_2SO_4.

3.2. Cyclic voltammetry

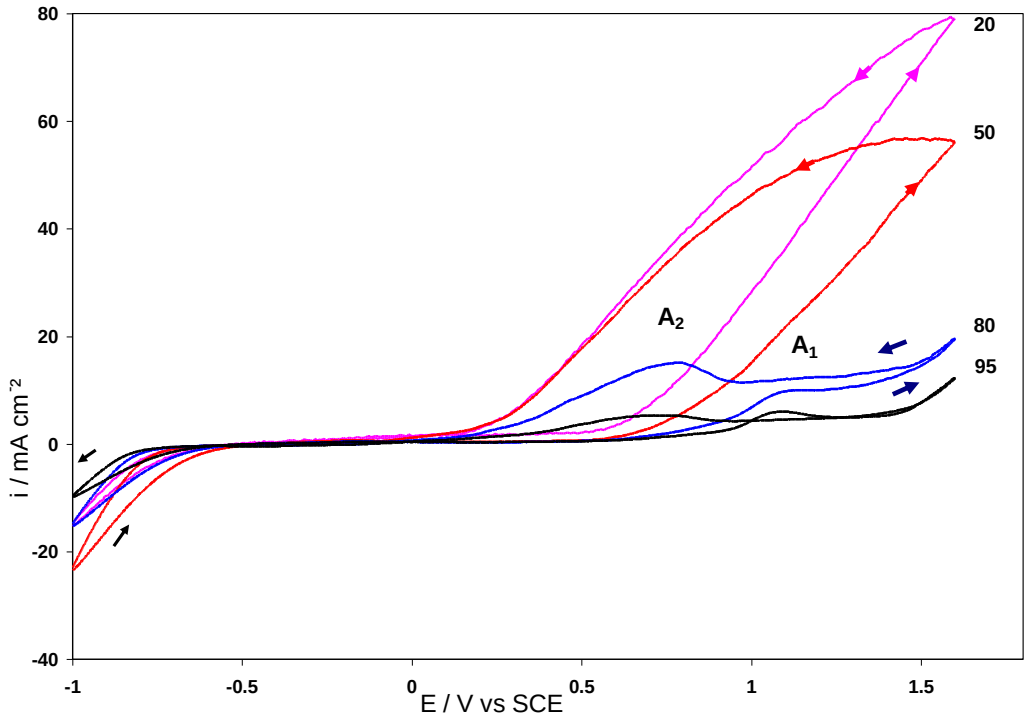

Figure 2. Selected cyclic voltammograms of an AISI 316 electrode in 0.1 N HCl run at 0.01 V s^{-1}. Cycle numbers are indicated in the figure.

Cyclic voltammograms (CVs) were run with stainless steel specimens at various pH, chloride and sulphate concentrations, potential sweep rates (v) and anodic ($E_{s,a}$) switching potentials to establish the potential ranges of the different electrochemical reactions of SS in the working solutions and their kinetic characteristics, and to select the most adequate conditions for the potentiostatic investigation of corrosion reactions.

Fig. 2 depicts the CVs of a steel electrode in 0.1 N HCl which were recorded by potential cycling the working electrode at 0.01 V s^{-1} between -1.00 and +1.60 V_{SCE}, up to 95 cycles. The CVs show the onset of hydrogen evolution reaction at potentials below -0.57 V_{SCE}. On the other hand, when the potential excursion in the positive direction exceeds E_{pit} = +0.50 V_{SCE}, the current rises suddenly to a very high value, indicating the breakdown of the passive film and the initiation of pitting corrosion of the steel electrode in 0.1 N HCl. This potential corresponds to the threshold of the transpassivation potential. E_{pit} values shift to more noble potentials with repeated cycling of the electrode between -1.00 and +1.60 V_{SCE}. In the potential range where anodic currents are observed, and for a given potential, the anodic currents measured in the negative-going sweep are somewhat bigger than those recorded during the previous forward scan, originating a hysteresis loop due to the activation of the electrode. This hysteresis is a characteristic of the pitting corrosion phenomenon, and it allows the repassivation potential to be determined from the cyclic voltammograms. The measured current tends to zero at the protection potential, E_{prot}, which occurs at ca. +0.24 V_{SCE} during the reverse scan. It represents the potential value below which no pitting occurs and above which pit nucleation starts. E_{prot} stands for the potential value at which the descending curve reached the zero current during the reverse scan.

The anodic current decreased gradually with increasing the number of successively repeated cycling up to the 50^{th} cycle while the cathodic currents were less sensitive to potential cycling of the electrode. The values of E_{pit} shift in the positive direction with cycling of the SS in the range from -1.00 to 1.60 V_{SCE}. Thus the passive layer becomes more protective due to thickening of the passive film as a result of the competition between the formation of soluble species and the formation of the metal oxy-hydroxydes at the electrode surface. After the 80^{th} cycle, the shape of the voltammograms changes in the positive potential range through the occurrence of a current plateau extending between +0.90 and +1.50 V_{SCE}, which is then followed by oxygen and chlorine evolution beyond +1.50 V_{SCE}. The decrease of the current plateau with cycling allows the appearance of a new current peak A1 at 1.10 V_{SCE} during the forward scan. The reverse scan shows a broad current peak A2 centered around +0.70 V_{SCE} and extending between +0.90 and +0.25 V_{SCE}. At this stage, the colour of the solution changed to yellow – green depending on the number of cycles. This colour change is attributed to the release of Fe^{3+} and Cr^{3+} ions into the solution owing to their characteristic yellow and green colourings, respectively [7].

In order to identify the reactions involved in the formation of the passive layer on the SS electrode, CVs were next run between the negative switching potential $E_{s,c}$ = -1.00 V_{SCE} and a value of $E_{s,a}$ progressively shifted in the positive direction up to $E_{s,a}$ = +1.60 V_{SCE}. It was revealed that the anodic peak A2 is only observed when the switching anodic potential reaches ca. +1.10 V_{SCE}, that is, in the potential region covered by peak A1. Under these conditions, the size of peak A2 was also observed to depend on the value of $E_{s,a}$ (results not shown in the figures). Therefore, it is likely that the

peak A2 can be assigned to the further oxidation of corrosion products formed in the potential range of peak A1.

Similar experiments were performed for AISI 316 specimens exposed to sulphuric acid environment. In this case, the shape of the voltammograms recorded for a steel electrode in 0.1 N H_2SO_4 is observed to be less affected by potential cycling between -1.00 and +1.60 V_{SCE} than it was in the case of the exposure of another sample to hydrochloric acid solution.

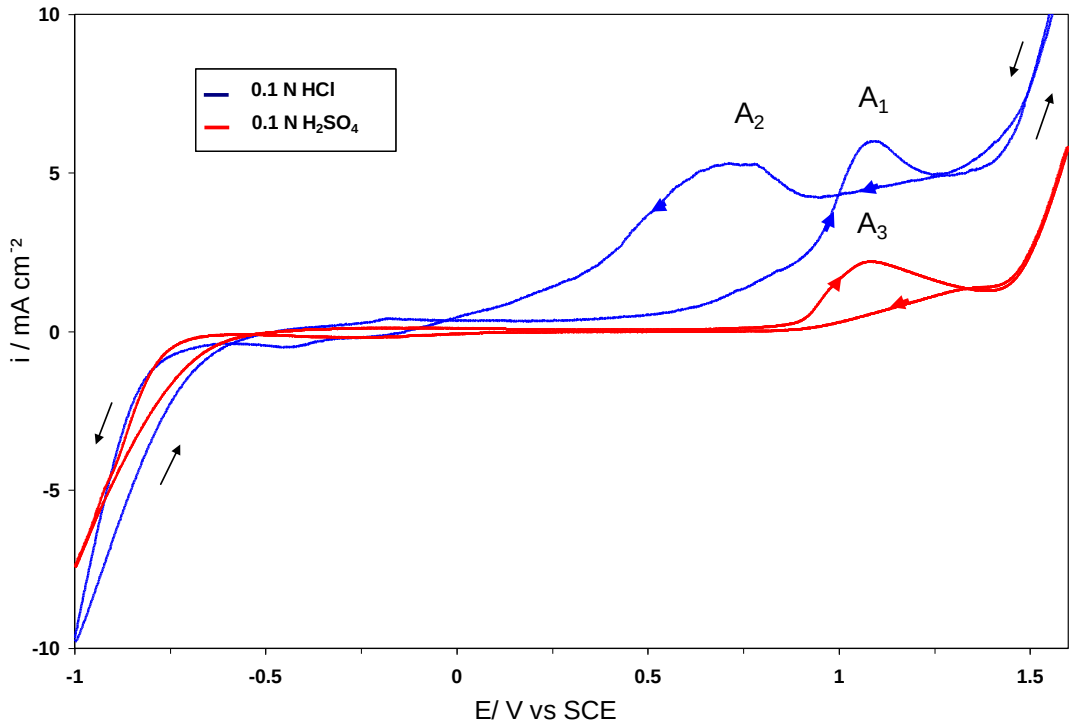

Figure 3. Cyclic voltammograms of AISI 316 electrodes. They correspond to the initial CV for the sample immersed in 0.1 N H_2SO_4 and to the 95th cycle for that in 0.1 N HCl; v = 0.01 V s^{-1}.

Fig.3 depicts the first cyclic voltammogram of a freshly prepared SS electrode immersed in 0.1 N H_2SO_4 recorded at a potential scan rate of 0.01 V s^{-1}. For the sake of comparison, the 95th CV obtained in 0.1 N HCl is also shown. The voltammogram obtained in 0.1 N H_2SO_4 exhibits a single current peak A3 in the same potential region where current peak A1 was observed for a SS sample exposed to 0.1 N HCl. The onset potentials related to SS oxidation which were recorded in the two solutions are very similar. However the height of the peak was smaller and no activation during the reverse potential scan was observed for the sample in the sulphuric acid solution. Additionally, no current peak is observed for the SS electrode in H_2SO_4 during the negative-going potential sweep in the potential range extending from +0.90 to +0.25 V_{SCE}, that is, in the potential region where peak A2 was observed in 0.1 N HCl.

The effect of the sweep rate on the shape of the voltammetric profiles of SS specimens immersed in either 0.1 N HCl or 0.1 N H_2SO_4 was investigated in the 5 to 50 mV s^{-1} range. Figs. 4 and 5 give some selected CVs in the two solutions.

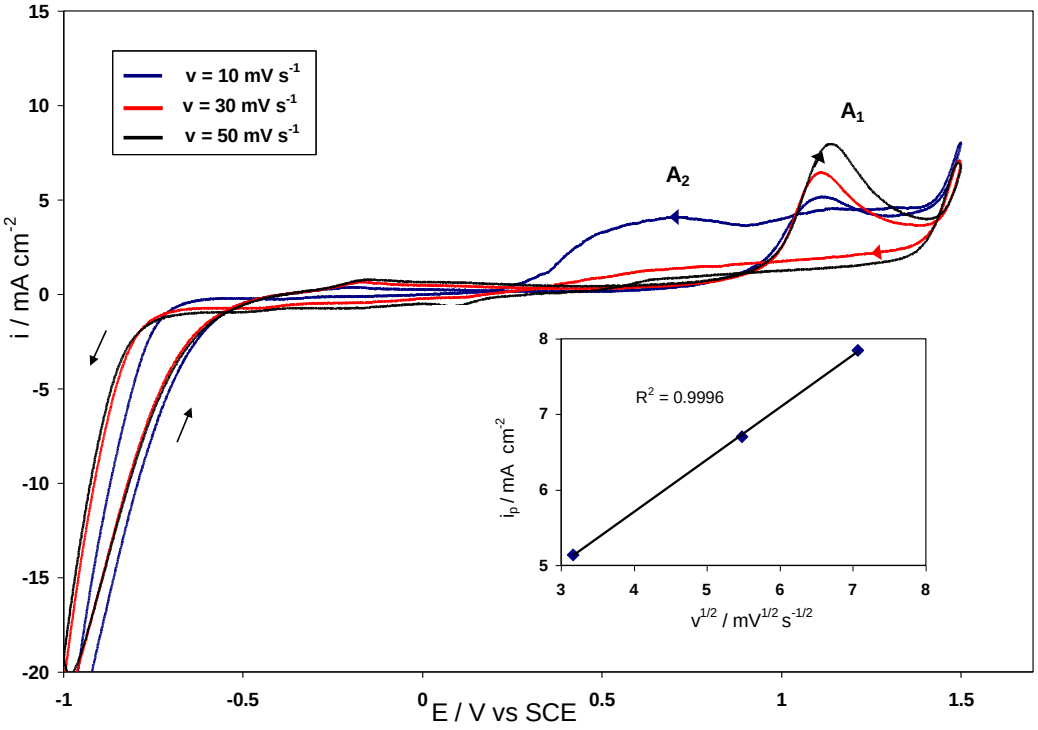

Figure 4. Cyclic voltammograms of an AISI 316 electrode in 0.1 N HCl at various potential scan rates as indicated in the figure. In the inset, current peak height versus $v^{1/2}$ relationship, where v is the scan rate, for anodic peak A1.

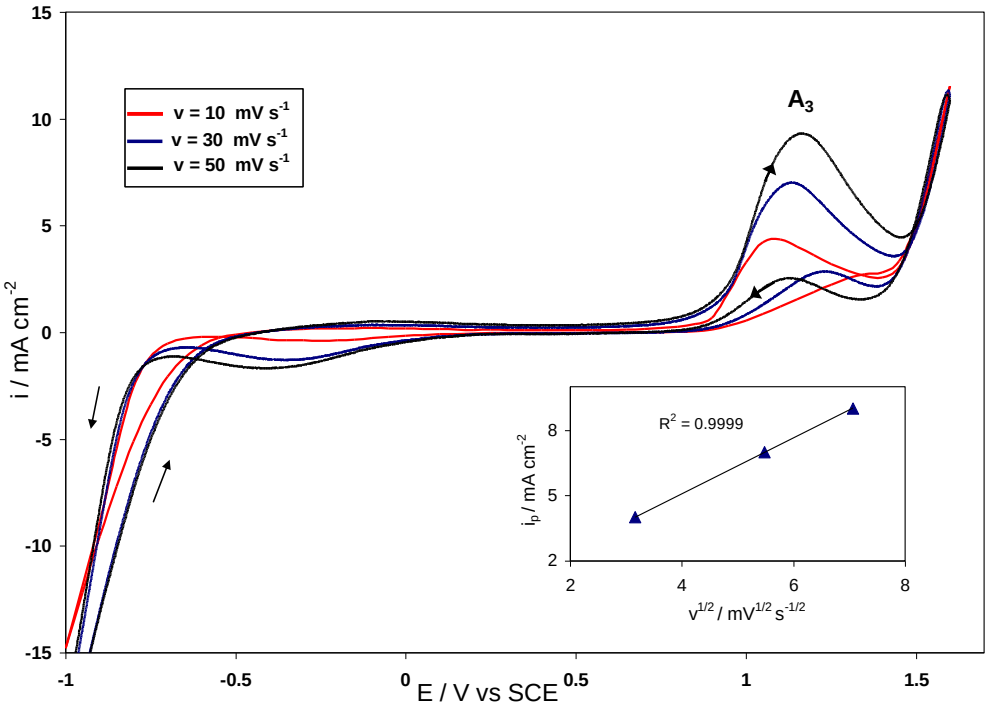

Figure 5. Cyclic voltammograms of an AISI 316 electrode in 0.1 N H_2SO_4 at various potential scan rates as indicated in the figure. In the inset, current peak height versus $v^{1/2}$ relationship, where v is the scan rate, for anodic peak A3.

In the case of the specimen immersed in 0.1 N HCl, and in the range of positive potentials, the peak current (i_p) for A1 increases, whereas peak current for A2 decreases, with the increase of the potential sweep rates. Indeed, for scan rates, v, faster than 0.03 V s^{-1}, peak A2 was totally absent from the CVs, and the current values measured in the reverse scan decreased drastically. On the other hand, in the 0.1 N H_2SO_4 solution, the height of the current peak A3 was higher as the potential sweep rate increased. It should be noted that in the negative going sweep, a small current peak corresponding to activation of the electrode is now observed. For peaks A1 and A3, the peak current approaches a linear dependence with $v^{1/2}$ (insets in Figs. 4 and 5) suggesting that there is a diffusion controlled process operating in both electrolytes. Additionally, the two peaks shift to more positive potential values as the potential is swept more rapidly. Finally, in the negative range of potentials, the cathodic currents decreased with increasing the sweep rates in both electrolytes.

The variation of pH does not seem to play a strong effect on the shape of the cyclic voltammograms as depicted in Figs. 6 and 7 for HCl and H_2SO_4 environments, respectively. Though the concentration of the acids were varied from 0.1 to 0.5 N, all the CVs exhibit the same features already observed in the diluted solution of concentration 0.1 N. Yet, it must be noticed that both the anodic peak current increases in height, and the peak potential values shift to nobler values, as the concentration of the acid is made higher. Also, the onset of the transpassive region is observed to be pH dependant.

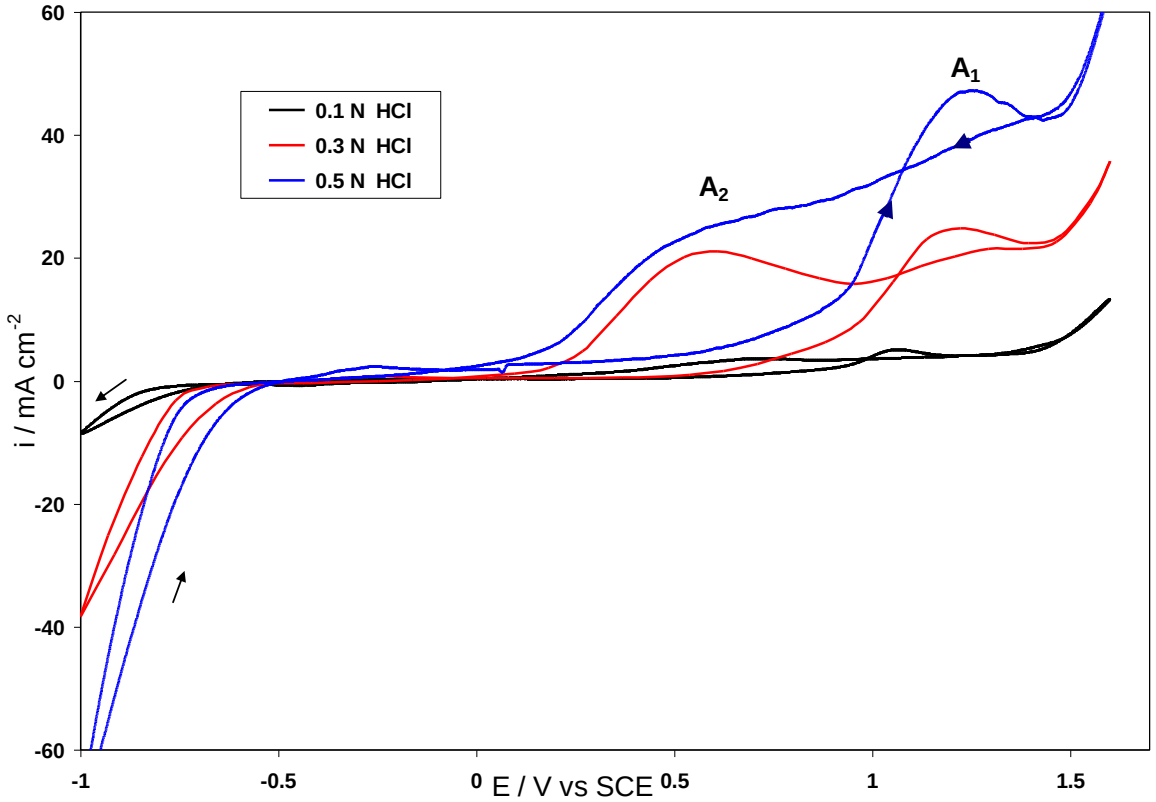

Figure 6. Cyclic voltammograms of AISI 316 electrodes in HCl solutions of different concentrations, as indicated in the figure; v = 0.01 V s^{-1}.

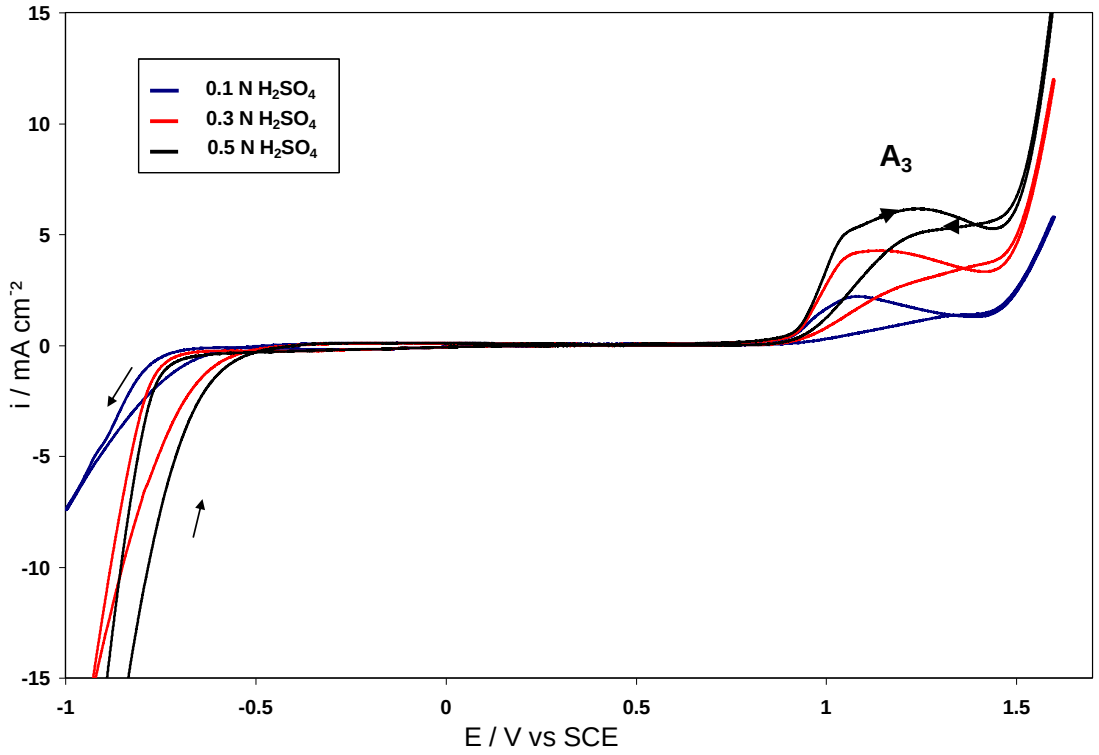

Figure 7. Cyclic voltammograms of AISI 316 electrodes in H_2SO_4 solutions of different concentrations, as indicated in the figure; v = 0.01 V s^{-1}.

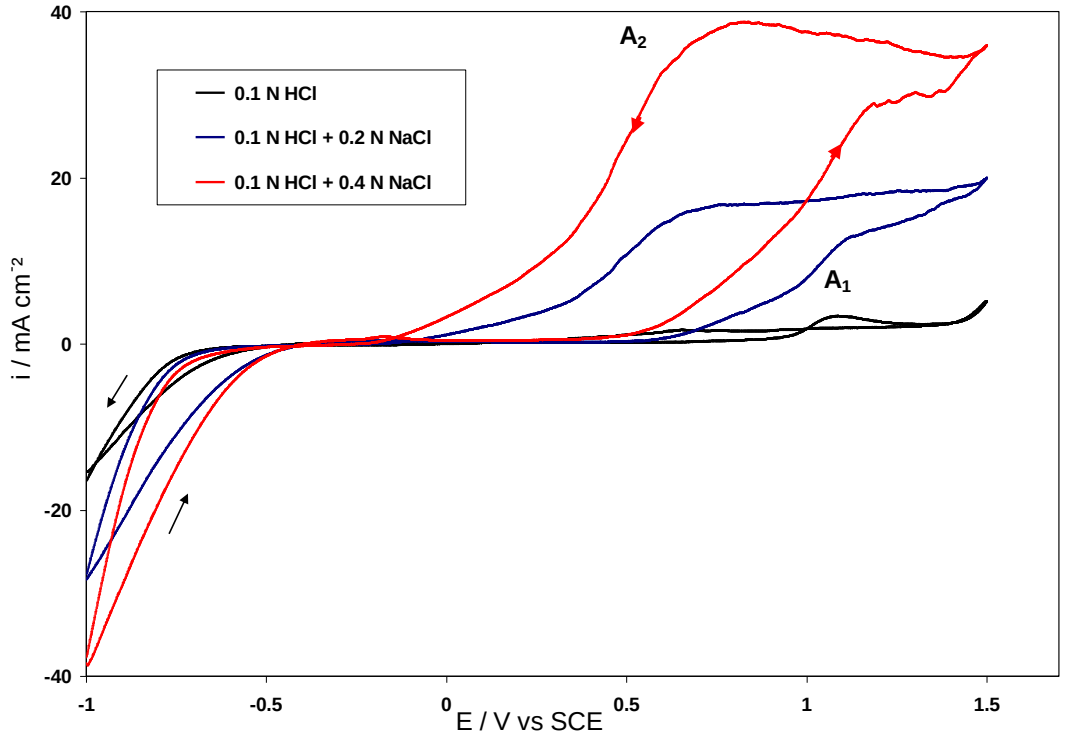

Figure 8. Cyclic voltammograms of AISI 316 electrodes in 0.1 N HCl solution containing 0, 0.2 and 0.4 N NaCl, respectively; v = 0.01 V s^{-1}.

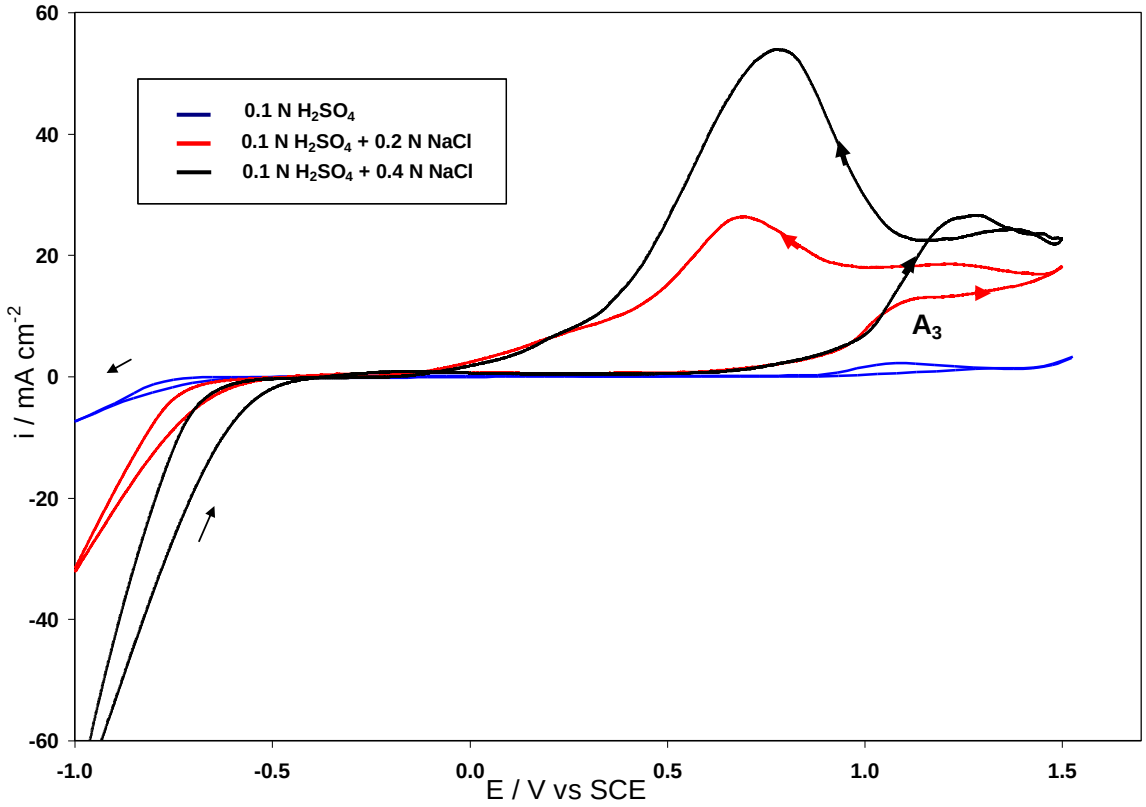

Figure 9. Cyclic voltammograms of AISI 316 electrodes in 0.1 N H_2SO_4 solution containing 0.1, 0.3 and 0.5 N NaCl, respectively; v = 0.01 Vs^{-1}.

For further investigating the effect of chloride ions on the susceptibility of 316 SS to pitting corrosion, a series of CVs were run for new SS specimens immersed in solutions consisting of controlled additions of NaCl to the base acid solutions of 0.1 N concentration, and they are shown in Figs. 8 and 9. In all cases, the addition of NaCl to acidic media affects the shape of the CV curves as it enhances the corrosion rate of the metal in the transpassivation region. It is worth noting that the CVs obtained in sulphuric acid containing NaCl exhibit a new peak during the extreverse scan which extends between +0.90 and +0.50 V_{SCE} which is due to the presence of chloride ions in the test environment. The oxidation currents determined from the steel sample immersed in hydrochloric acid solution are higher than those measured in sulphuric acid solution for a given total chloride ion concentration in the electrolyte. Such behaviour is due to the establishment of a combined aggressive effect of acidity and chloride ions which compensate the passivating characteristics of sulphate ions. Similar results have been reported for AISI 304 austenitic stainless steel in methanolic solution of hydrochloric acid to which sulphuric acid was added [7]

The voltammetric data confirm that the corrosion resistance of 316 austenitic stainless steel greatly depends on both the nature and the concentration of the acidic solution, though the passive film of AISI 316 stainless steel is mainly composed of oxides and hydroxides of Fe(II), Cr(III) and Mo(VI) [8]. Thus, the corrosive attack of SS leading to the formation of pits is favoured by the increase in the polarisation of the electrode, the increase of chloride concentration in the solution (either using higher

HCl concentrations or additions of NaCl to the electrolyte), or by decreasing the potential scan rate pit attack is significantly favoured. Consequently, bare steel is subject to corrosion activation. On this basis, the improvement of the corrosion behaviour of the stainless steels could be observed particularly from the disappearance of current peak A2 with increasing scan rate and the activation of the SS electrode in the reverse scan in solutions containing chloride ions.

3.3. Chronoamperometry

Potentiostatic current transients (i.e., chronoamperograms) were recorded at constant potential for SS samples immersed in 0.1 N HCl solution, and they were plotted as current density vs. time plots. The anodic current were run by setting the potential at different E_s values located in the potential range between +0.50 and +1.50 V_{SCE} for 30 min. Fig. 10a and 10b give the measured current transients in both linear and logarithmic scales, respectively. For $E_s \leq +0.90$ V_{SCE}, the current transients showed a monotonous increase of the current density values with the elapse of time as depicted in Fig. 10a. This continuous increase of the current densities with time is due to the propagation of the already nucleated pits forming stable pits [9].

In the case of the specimens polarized at more active potential values, $E_s > +0.90$ V_{SCE}, three separate zones can be distinguished from the current transients in Fig. 10a. The transients show an initial decrease of the anodic current (zone I), and then an increase up to a maximum value I_M at time t_2 (zone II), and finally a monotonous decrease (zone III).

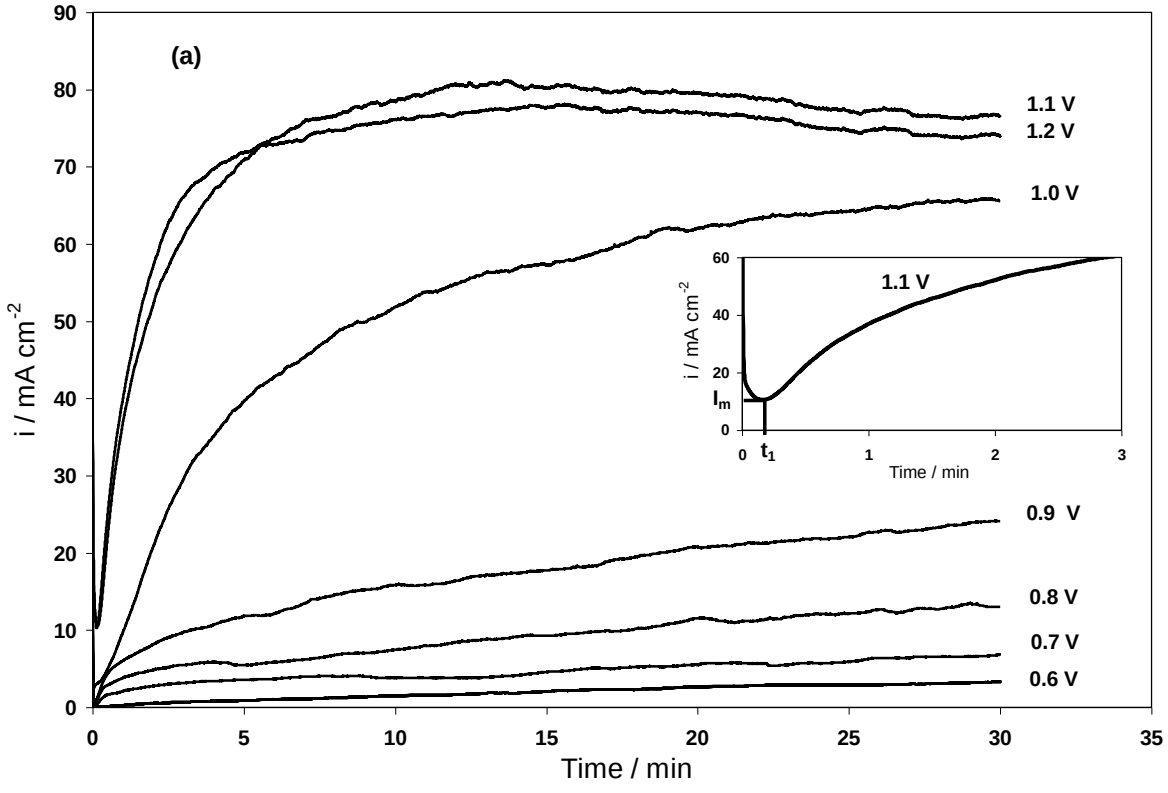

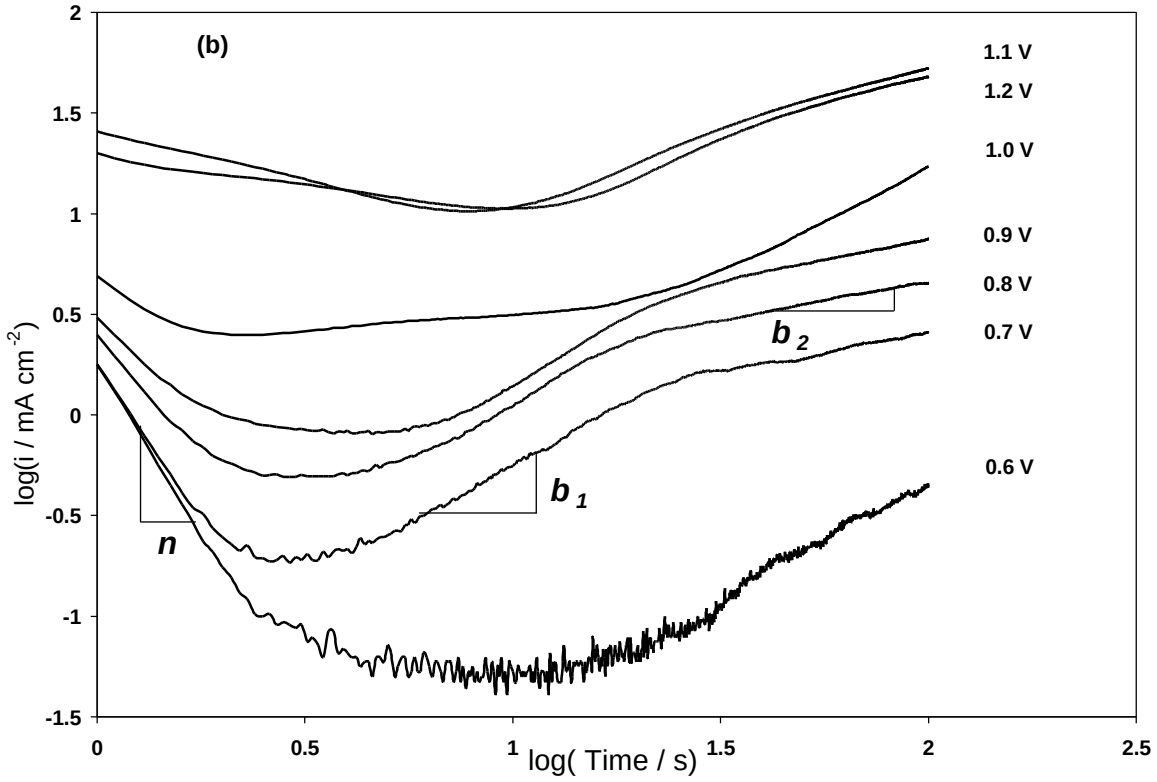

Figure 10. Potentiostatic current transients for AISI 316 electrodes in 0.1 N HCl, using linear (a) and logarithmic (b) scales. Inset in (a) corresponds to a detail of the initial portion of the transient recorded for E_s = 1.10 V. Slopes n, b_1 and b_2 in (b) are related to the rate of growth of the passive layer, the stages of pit nucleation and of pit growth, respectively. E_s values are indicated in the figure.

The inset in Fig. 10a allows zones I and II to be clearly distinguished in the transient recorded for E_s = +1.10 V within the first 3 min of the potential application to the working electrode. From the curve in the inset, the minimum in the current transient can be characterized through the minimum current density I_m and the corresponding time t_1, which represents an induction time. The first zone corresponds to the initial abrupt decrease of current density with time and subsequent attainment of a current density minimum at time t_1, which is an induction time. Park and Pyun [10] attributed this initial part to the first passivation stage where thickening of the passivation film is reached at t_1. The reciprocal of the induction time $(t_1)^{-1}$ corresponds to the rate of pit nucleation. The decrease of the initial current density is related to the growth of the passive film on the electrode. Macdonald and coworkers [11,12] fitted the growth of the passive film using the equation:

$$i = A(t)^{-n} \quad (1)$$

where i is the current density, and A and n are parameters which depend on the applied potential values and the electrolyte composition. In this equation, n stands for the rate of growth of the passive layer. By plotting the current transients in logarithmic scales, linear relationships can be

extracted in various regions of the curves. The values of slopes *n* for the first straight line in Fig 10b, which occurs at the shortest times, are listed in Table 2, and they are observed to decrease with the shift of the applied potentials to more positive values, which stands for a decrease in the growth rate of the film at higher potentials. Both the pit nucleation rate, $(t_1)^{-1}$, and the current density value in the minimum of the current transient, I_m, increased with the application to the electrode of higher potentials up to +1.10 V_{SCE}, whereas they decreased beyond that value.

Table 2. Parameters used in simulation of potentiostatic current transients with equations (1) and (2).

E_s / V_{SCE}	n	b_1	b_2	t_1^{-1} / s^{-1}	I_m / mA cm^{-2}
+0.60	3.4	-	0.9	0.10	0.04
+0.70	3.1	0.9	0.4	0.20	0.18
+0.80	2.4	1.2	0.4	0.34	0.50
+0.90	1.8	1.2	0.4	0.35	0.81
+1.00	1.4	0.9	1.0	0.40	2.50
+1.10	0.5	0.9	0.6	0.10	10.60
+1.20	0.5	0.9	0.5	0.13	10.30

The second portion of the chronoamperometric curves, Fig 10a, that extends from t_1 to t_2, and corresponds to the portion of the transient where the current increased, was attributed to film breakdown due to the nucleation of pits. Finally, the third portion, where the current decreases continuously before reaching the steady state, would correspond to the growth of pits [9, 10]. The measured current densities were fitted by using the Engell-Stolica's [13] relationship:

$$i = B(t)^b \qquad (2)$$

where *B* and *b* are parameters which depend on the applied potential values and the electrolyte composition.

From the inspection of Fig. 10b, the curves can be approximately reproduced using only two straight lines with slopes b_1 for the first line, and b_2 for the second one, when times longer than t_1 are considered. This observation could be explained by assigning b_1 and b_2 to pit nucleation and pit growth stages, respectively [14]. The data reported in Table 2 show that b_1 remained almost constant whereas b_2 increased with applied potentials up to +1.00 V_{SCE}, and they decreased at more positive values. For each applied potential, the steady state was reached when the formation of oxide film on the steel electrode was compensated by pitting corrosion after the time t_2. The steady state current increased as the applied potential was set less positive than $E_s \leq +1.10$ V_{SCE}, and decreased at higher potential values. These results could be explained by the preponderance of the pitting corrosion process for the

potentials beyond +1.10 V_{SCE}, whereas the blockage of pits by the precipitation of corrosion products would occur at more positive potentials.

4. CONCLUSION

The electrochemical behaviour of austenitic 316 stainless steel in acidic solutions depends considerably on the concentration of chloride ions and the acidity of the environment. The presence of chloride ions produces and enhancement of metal corrosion through the passive layer, and decreases the passivity breakdown potential. Pit nucleation and growth involves a number of contributions which can be distinguished through the analysis of current transients at constant potential by using the procedure derived by Engell and Stollica [13].

ACKNOWLEDGEMENTS
The authors gratefully acknowledge the support of this work by the Pôle de Compétences Electrochimie-Corrosion et Chimie Analytique (PECCA), Ministère de l'Education Nationale, de l'Enseignement Supérieur, de la Formation des Cadres et de la Recherche Scientifique.

References

1. H. Alves, D.C. Agarwal, H. Werner, Nace - International Corrosion Conference Series, 2006, Houston, 62221
2. A.Pardo, M.C. Merino, A.E. Coy, F. Viejo, R. Arrabal, E. Matykina, *Corros. Sci*.50 (2008) 780
3. M.G. Fontana, N.D. Greene, Corrosion Engineering, 1967, McGraw-Hill, New York, 51
4. M.E. Curley-Fiorino, G.M. Schmid, *Corros. Sci*. 20 (1980) 313
5. S.A.M. Refaey, F. Taha, A.M. Abd El-Malak, *Int. J. Electrochem. Sci*.1 (2006) 80
6. H.A. Aldahan *J. Mater. Sci*. 34 (1999) 851
7. V.B. Singh, M. Ray, *Int. J. Electrochem. Sci.* 2 (2007) 329
8. A. Pardo, M.C. Merino, A.E. Coy, F. Viejo, R. Arrabal, E. Matykina, *Corros. Sci*. 50 (2008) 1796
9. H.H. Hassan, K. Fahmy, *Int. J. Electrochem. Sci*. 3 (2008) 29
10. J.-J. Park, S.I. Pyun, *Corros. Sci.* 45 (2003) 995
11. D.D. Macdonald, M.J. Urquidi-Macdonald, *J. Electrochem. Soc*. 137 (1990) 2395
12. C.Y. Chao, L.F. Lin, D.D. Macdonald, *J. Electrochem. Soc*.128 (1981) 1187
13. H.J. Engell, D.N. Stolica Z. *Phys. Chem. Unterr.* 20 (1959) 113
14. I.Milosev, M. Metikos-Hukovic, *J. Electrochem. Soc*. 138(1991) 61